

PACS numbers: 79.20.Ds; 52.38.Mf; 81.05.Uw
DOI: 10.1070/QE2014v044n06ABEH015455

Generation of negative pressures and spallation phenomena in diamond exposed to a picosecond laser pulse

S.A. Abrosimov, A.P. Bazhulin, A.P. Bol'shakov, V.I. Konov, I.K. Krasyuk, P.P. Pashinin, V.G. Ral'chenko, A.Yu. Semenov, D.N. Sovyk, I.A. Stuchebryukhov, V.E. Fortov, K.V. Khishchenko, A.A. Khomich

Abstract. **The spallation phenomena in poly- and single-crystal synthetic diamonds have been experimentally investigated. A shock-wave impact on a target was implemented using a 70-ps laser pulse in the Kamerton-T facility. The ablation pressure of 0.66 TPa on the front target surface was formed by pulsed radiation of a neodymium phosphate glass laser (second harmonic λ = 0.527 μm, pulse energy 2.5 J) with an intensity as high as 2×10^{13} W cm^{-2}. The maximum diamond spall strength $\sigma^* \approx$ 16.5 GPa is found to be 24% of the theoretical ultimate strength. Raman scattering data indicate that a small amount of crystalline diamond in the spallation region on the rear side of the target is graphitised.**

Keywords: *laser radiation, picosecond duration, ablation pressure, shock wave, negative pressure, spallation phenomenon, strain rate, ultimate strength, numerical simulation, synthetic diamond.*

1. Introduction

The study of the extreme states of materials at high strain rates is based on the shock-wave technique [1, 2]. Generation of shock waves in materials irradiated by short high-power laser pulses [3–6] provided a large amount of experimental data on the properties of metals, ceramics, glass, polymers and other materials under high (to several tens of gigapascals) pressures; in particular, their dynamic strength (which significantly exceeds the static strength) was measured in [5, 6]. An important phenomenon of shock-wave dynamics in a loaded material is the effect of spallation of a target layer on the rear (free) side of the target due to the reflection of a pressure pulse formed in a particular way on the front target surface [7]. The free target surface starts moving, due to which an extension wave propagates toward a compression wave. At some distance from the rear surface the pressure in the target may become negative and the tensile stress may exceed the ultimate strength of the target material; as a result, a spallation layer is formed to be detached and flown away from the target. The interest in the behaviour of matter under negative pressures is due to the possibility of gaining a deeper insight into the equations of state, phase transitions, polymorphic transformations and mechanisms of fracture of material under tensile loads in the regions of phase diagrams that have not been studied to date [1]. Currently, the most interesting subject is the use of picosecond and femtosecond laser pulses, which provide a short-term impact.

In this context, it is of great interest to analyse the behaviour a unique material – diamond – under high dynamic pressures (formed by a shock wave) and its ultimate strength. Diamond has a set of record physical characteristics: concentration of atoms (1.78×10^{23} cm^{-3}), Debye temperature (1860 K), hardness (80–140 GPa), Young modulus (1050 GPa), thermal conductivity (~2000 W mK^{-1}), longitudinal speed of sound (18.4 km s^{-1}), and transparency window (from 225 nm to the radio wavelength range). The static breaking strength of diamond single crystals is 2.8 GPa [8]. Diamond anvils were used to obtain the highest static pressures: up to 0.2 TPa [9].

In this paper, we report the results of experimental study of the specific features of spallation phenomena in poly- and single-crystal diamond targets in the range of negative pressures under a shock-wave impact formed by a 70-ps laser pulse. Experimental data on the dynamic tensile strength of these materials were obtained for the first time. As far as we know, the spallation mechanism of diamond fracture has not been investigated previously. The phase transitions of carbon in the spallation plane were studied by Raman spectroscopy.

2. Experimental conditions

The experiments were performed on the Kamerton-T facility based on a neodymium phosphate glass laser at the A.M. Prokhorov General Physics Institute, Russian Academy of Sciences. We used second-harmonic radiation with a wavelength 0.527 μm. A pulsed laser beam with a pulse energy of 2.5 J was focused on a target into a spot from 0.3 to 0.8 mm in diameter. The maximum beam intensity in the focusing region reached 1.9×10^{13} W cm^{-2}; the ablation pressure was 0.66 TPa. The parameters of the laser radiation and materials under study are listed in Table 1. The vacuum chamber was equipped with an automatic three-coordinate target unit and a two-component objective for controlling the laser radiation intensity on the target. The laser beam transmission through the diaphragms of spatial filters was monitored using a computer-assisted video system. A schematic of the experiments is shown in Fig. 1.

Samples (polycrystalline diamond plates) were synthesised by chemical vapour deposition in a microwave discharge (2.45 GHz) in a plasma-chemical UPSA-100 reactor (Optosystems Ltd.) in $CH_4-H_2-O_2$ mixtures [10, 11]. Opaque (black) diamond films with thicknesses from 140 to 400 μm were

S.A. Abrosimov, A.P. Bazhulin, A.P. Bol'shakov, V.I. Konov, I.K. Krasyuk, P.P. Pashinin, V.G. Ral'chenko, A.Yu. Semenov, D.N. Sovyk, I.A. Stuchebryukhov, A.A. Khomich A.M. Prokhorov General Physics Institute, Russian Academy of Sciences, ul. Vavilova 38, 119991 Moscow, Russia; e-mail: krasyuk@kapella.gpi.ru, abr@kapella.gpi.ru;
V.E. Fortov, K.V. Khishchenko Joint Institute of High Temperatures, Russian Academy of Sciences, ul. Izhorskaya 13/2, 125412 Moscow, Russia

Received 3 March 2014; revision received 12 March 2014
Kvantovaya Elektronika **44** (6) 530–534 (2014)
Translated by Yu.P. Sin'kov

Table 1. Parameters of radiation and diamond samples.

Sample number	Shot number	D_{inp} /mm	E /J	$I/10^{13}$ W cm^{-2}	P /TPa	H_0 /μm
I (unpolished black diamond)	1	0.405	1.710	1.72	0.61	320
	2	0.314	1.155	1.93	0.66	320
II (unpolished white diamond)	1	0.81	0.75	1.75	0.11	300
	2	1.04	2.84	4.3	0.24	300
III (polished white diamond)	1	0.73	1.5	4.6	0.24	260
	2	0.83	2.88	6.9	0.31	260
	3	0.83	2.61	6.3	0.29	260
IV (one-side-polished black diamond)	1	0.46	0.48	3.7	0.20	400
	2	0.46	0.69	5.4	0.26	400
	3	0.46	1.00	7.8	0.33	400
V (one-side-polished black diamond)	1	0.65	0.57	2.23	0.135	150
VI (one-side-polished black diamond)	1	0.61	1.66	7.4	0.32	140
	2	0.61	1.33	5.9	0.28	140
VII (single-crystal diamond)	1	0.822	1.50	3.6	0.20	266
	2	0.822	2.37	5.8	0.277	315

Note: D_{inp}, E, I, P and H_0 are, respectively, the laser spot diameter, laser pulse energy, irradiation intensity, ablation pressure in the irradiation spot, and target thickness.

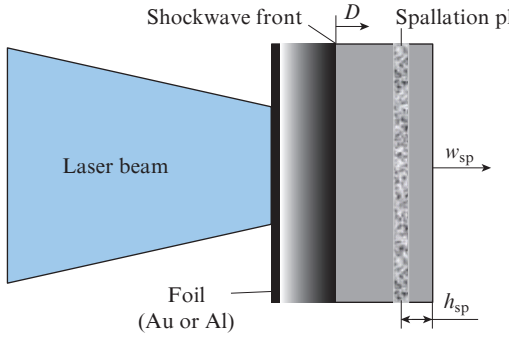

Figure 1. Schematics of laser impact on a diamond target (D is the shock-wave front velocity and w_{sp} and h_{sp} are, respectively, the velocity and thickness of spallation plate).

deposited on silicon substrates 57 mm in diameter under the following technological conditions: working mixture $CH_4:O_2:H_2 = 10:1:89$, pressure 95–100 Torr, total gas consumption 1 L min^{-1}, and substrate temperature 940 °C. Transparent films about 300 μm thick were grown in a $CH_4:H_2 = 1.5:98.5$ mixture at a lower temperature (820–850 °C). After etching off the silicon substrate, the diamond films were cut by a Nd:YAG laser beam into plates with sizes from 5×5 to 8×8 mm. The polycrystalline plates had an anisotropic structure: they consisted of column-like crystallites with axes oriented perpendicular to the plate plane. The grain size was ~ 1 μm at the substrate side and increased to several tens of micrometers at the opposite (growth) side. Although crystallites form a fairly rough surface at the growth side, only one of the samples was polished from this side. To implement the spallation effect, laser irradiation of diamond plates was always performed from the smooth (substrate) side, which had a roughness $R_a \sim 10$ nm.

Targets of other types were commercially produced plates of single-crystal synthetic diamond (Ib type) of (100) orientation, grown at high pressures; they were polished and had a thickness of about 300 μm.

The morphologies of the front and rear surfaces of the samples subjected to laser irradiation were investigated with a scanning electron microscope (SEM). The relief of the fracture region and the depth of the craters formed on both sample sides were measured with a NewView 5000 optical profilometer (Zygo). The phase composition of the material on the irradiated and spallation target surfaces and on the collected cleaved fragments that flew away were analysed by Raman spectroscopy on a LabRam HR spectrometer (Horiba) with a spectral resolution of 0.5 cm^{-1}; in this case, a 0.488-μm laser beam was focused into a spot ~2 μm in diameter on the sample surface. To minimize the volume of material analysed, we applied a confocal optical scheme with a slit width of 100 μm.

3. Method for determining the spall strength and strain rate

To determine the spall strength σ^* and strain rate $\dot{V}/V_0$ of a medium (here, V_0 is the initial specific volume and $\dot{V}$ is the rate of its change in time), we used an approach based on measuring the depth of spallation groove h after pulsed irradiation of the target, with subsequent mathematical simulation of the shock-wave process in the sample [12, 13]. The σ^* and $\dot{V}/V_0$ values were calculated using a numerical code developed according to the Courant–Isaacson–Rees scheme based on hydrodynamics equations [14]. This code uses the wide-range semiempirical equation of state of diamond [15]. It was assumed that the ablation pressure pulse on the front target surface has the same shape as the laser pulse. The amplitude P_a of the ablation pressure pulse (in TPa) and the laser radiation intensity I_{las} (W cm^{-2}) were related by the semiempirical formula [16]

$$P_a = 1.2\,(10^{-14} I_{las})^{2/3} \lambda^{-2/3} [A/(2Z)]^{3/16}$$

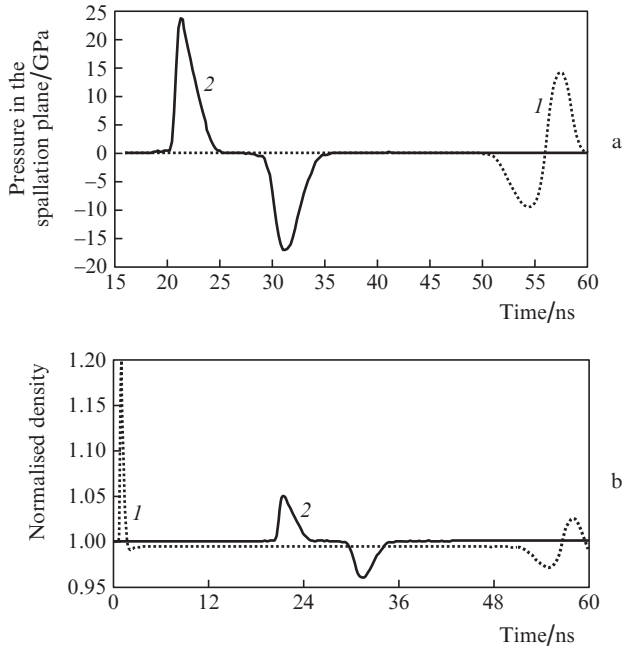

Figure 2. Calculated time dependences of (a) pressure and (b) normalised density of material in the spallation plane on the (*1*) front and (*2*) rear sides of target at distances of, respectively, 13 and 266 μm from the front target surface. The amplitude of ablation pressure pulse is 0.66 TPa.

at $I_{las} \geqslant 10^{12}$ W cm^{-2}, where λ is the laser radiation wavelength (μm) and A and Z are, respectively, the atomic weight and number of the target material.

In our experiments we fixed the intensity I_{las} at which spallation occurred. The spallation (tensile) strength at threshold shock-impact amplitudes was considered to be the minimum pressure modulus (negative in absolute value) in the spallation plane: $\sigma^* = |P_{min}|$. The results obtained in one of the calculation versions are shown in Fig. 2. The strain rate was found from the calculated time dependence of density $\rho(t)$ (Fig. 2b) by differentiating it with respect to time: $\dot{V}/V_0 = |\dot{\rho}(t)/\rho_0|$.

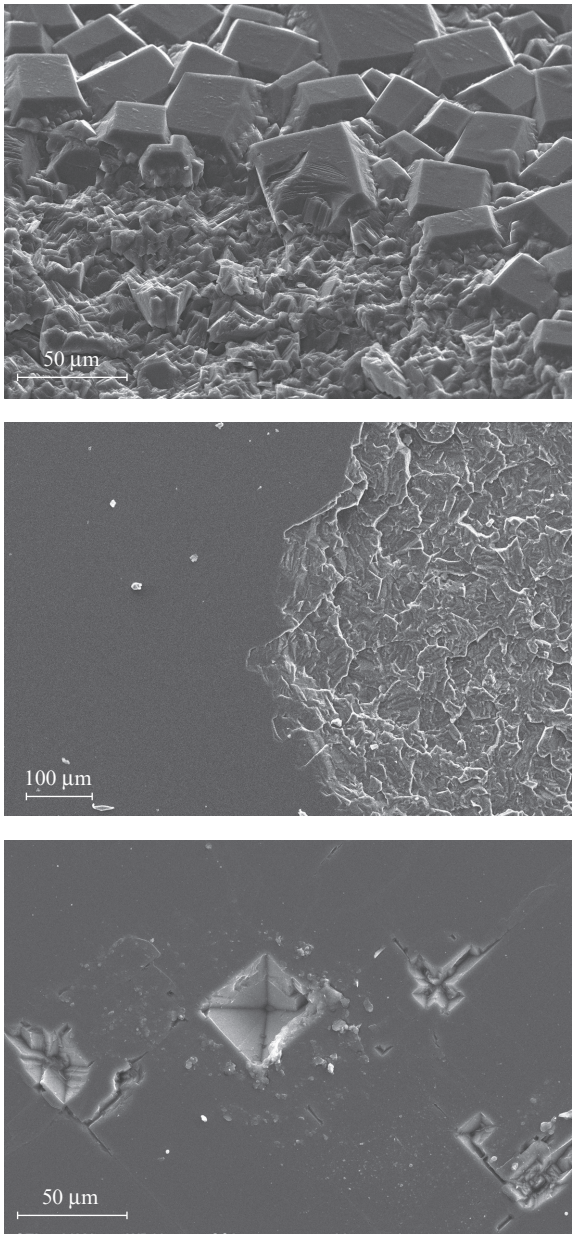

Figure 3. SEM images of the spallation surfaces of diamond targets: edges of craters in (a) 320-μm-thick unpolished black and (b) 260-μm-thick polished transparent polycrystalline diamond samples (the ablation pressure amplitudes at the front target surfaces are 0.66 and 0.31 TPa, respectively); (c) a 315-μm-thick single-crystal diamond sample [face (100), the ablation pressure amplitude at the front target surface is 0.28 TPa].

4. Experimental results

4.1. Target surface morphology

Figure 3 shows SEM images of rear (spallation) sides of the polycrystalline samples and single-crystal sample after shock-wave impacts with amplitudes of 0.66, 0.31, and 0.28 TPa, respectively. One can see a significant difference in the behaviour of poly- and single-crystal diamond samples under extension. Spallation of polycrystalline material occurs almost uniformly over all surfaces of spallation craters with maximum depths of 54.5 and 70 μm. The bottom of these craters has a fairly rough surface in comparison with the smooth rectangular (100) faces of initial (located beyond craters) crystallites 20–30 μm in size. This roughness is caused by the break of diamond over grain bulk rather than over grain boundaries [11].

The spallation in the single-crystal sample (Fig. 3c) is localised; separate fragments of pyramidal shape with cross-sectional areas from 20 to 40 μm are detached from the spallation region; the depth of the grooves is ~30 μm. The side faces of inverted pyramids are formed by the (111) planes, which are cleavage planes in diamond (i.e., they are most easy to cleave). A continuous crater was not formed, apparently, because the irradiation conditions were close to the fracture threshold. A dependence of the maximum depth of spallation crater on the laser pulse energy density is shown in Fig. 4. In polycrystalline diamond, the spallation-layer thickness tends to increase with an increase in the energy density; this tendency is less pronounced for the single crystal.

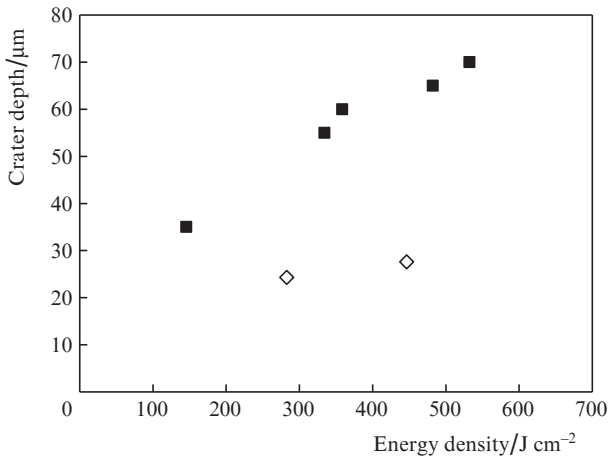

Figure 4. Dependences of the maximum depth of spallation crater on the energy density in laser pulse for (■) transparent polycrystalline and (◇) single-crystal diamond samples.

Figure 5 shows an SEM image of the cross section (cleavage) of a black polycrystalline diamond target 320 μm thick, in which both an ablation crater on the top (front side) and a spallation crater of somewhat larger diameter on the opposite side can clearly be seen. The maximum depth of the spallation crater is ~20 μm. In some cases spallation was observed not only on the rear side of the target but also on the front side. This behaviour is apparently caused by the successive effect of the ablation pressure pulse with an amplitude of 0.66 TPa on the front target surface and (after 50 ns) a negative (tensile) pressure pulse with an amplitude of 10 GPa. A detailed analysis

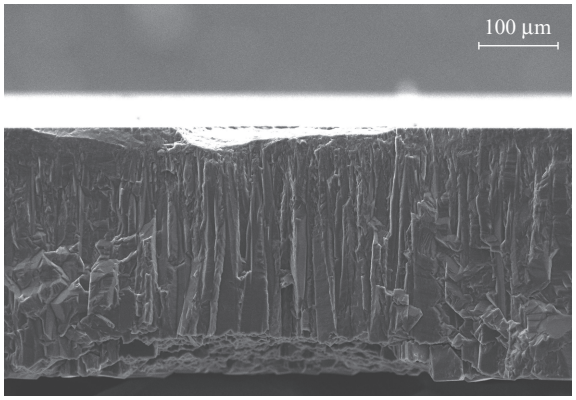

Figure 5. SEM image of a cleavage surface in a polycrystalline black diamond target, in which the crater diameter lies (the ablation and spallation craters are on the top and bottom, respectively). The ablation pressure amplitude on the front target surface is 0.66 TPa. The image of the spallation target surface is shown in Fig. 3a.

of this phenomenon, observed under certain conditions not only in diamond but also in aluminum, lead and graphite [5], will be published elsewhere.

4.2. Dependence of the spall strength of diamond samples on the strain rate

Figure 6 shows dependences of the spall strength σ^* of poly- and single-crystal synthetic diamonds on the strain rate $\dot{V}/V_0$. The data for the samples of both types are described by a unified curve given by the expression $\sigma^* = 1.17\times10^{-6}(\dot{V}/V_0)^{0.915}$. The errors in determining the spall strength σ^* and strain rate $\dot{V}/V_0$ are mainly related to the finite width of the spallation region. An analysis of the obtained experimental data and calculation results shows that maximum error in determining the spall strength and strain rate are 14% and 20%, respectively. A spall strength $\sigma^* \approx 16.5$ GPa was reached, which amounts to only 24% of the limiting theoretical value (69.5 GPa) yielded by the equation of state of diamond [15], but greatly exceeds the static breaking strength of diamond. For comparison, the breaking strength σ for similar polycrystalline diamond plates with thicknesses of 140–400 μm is 0.4–0.5 GPa [11].

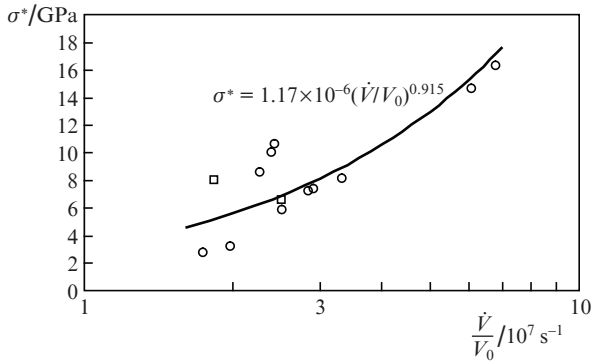

Figure 6. Dependences of the spall strength of (○) polycrystalline and (□) single-crystal diamond samples on the strain rate.

4.3. Phase transformations of carbon in spallation planes

Traces of sample surface graphitisation were sought for by Raman spectroscopy within ablation and spallation craters, as well as on collected fragments (spallation products). We investigated only transparent polycrystalline diamond, because in this case inclusions of amorphous graphite-like carbon in the initial (unirradiated) material are reduced to minimum. The sample was an unpolished diamond plate 4×8 mm in size and 300 μm thick (Table 1, sample II). One can clearly see distinctly faceted crystallites on the growth surface (which is rear with respect to the laser-irradiated side); these crystallites are responsible for the significant surface roughness. Irradiation was performed from the smooth (front) side, covered by a gold leaf film. Two craters were formed on the front target side after two laser shots with energies $E = 0.8$ and 2.8 J; the higher energy corresponds to the larger crater. These energies correspond to ablation pressures of 0.11 and 0.24 TPa, respectively. Two craters were also formed on the rear side of the target as a result of spallation.

The Raman spectrum recorded beyond the laser-irradiated region ($E = 2.8$ J) on the fine-grained substrate side of the target contains a dominant narrow peak of diamond near 1332.5 cm^{-1} [Fig. 7, spectrum (*1*)]. There is also a very weak wide G band in the range of 1500–1530 cm^{-1}, which is only indicative of low content of amorphous carbon in the sample. The Raman spectrum recorded in the ablation crater contains wide D and G bands near 1350 and 1550–1590 cm^{-1}, respectively, which indicate formation of disordered graphite phase in rather large amounts [Fig. 7, spectrum (*2*)]. Similar results were obtained for the small crater ($E = 0.8$ J).

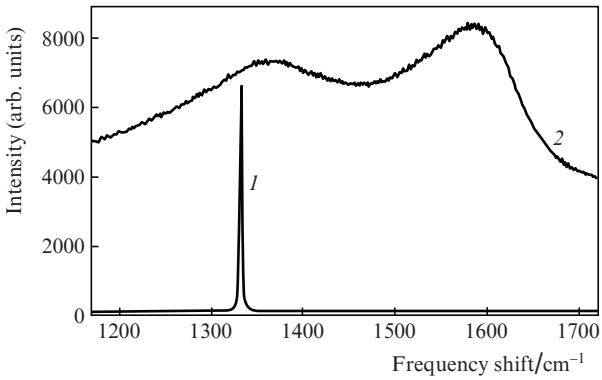

Figure 7. Raman spectra of the (*1*) initial (intact) region and (*2*) a region within the ablation crater in a transparent polycrystalline diamond sample on the substrate (ablation) side (the pulse energy is $E = 2.8$ J).

For comparison, Fig. 8 shows the Raman spectra of the initial target material (Table 1, sample III, shot 2) on the coarse-grained (spallation) side [spectrum (*1*)] and fragments of spallation plate [spectrum (*2*)]. The knocked-out material flew away from the rear target surface in the form of a compact set of fragments. Fragments were collected on a scotch tape located behind the irradiated plate. The spectrum of fragments contains, along with the diamond line, pronounced D and G lines near 1350 and 1590 cm^{-1}, respectively. The intensities of all lines were amplified in order to observe weak lines of the graphite-like phase; the total Raman spectrum of the same fragment is shown in the inset in Fig. 8. The spectra were normalised to the total intensity of the diamond line to con-

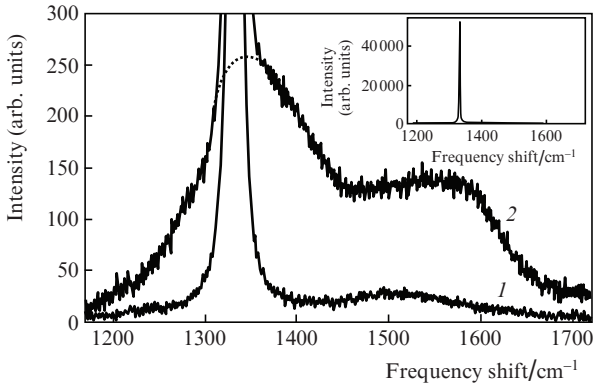

Figure 8. Raman spectra of the (*1*) initial (intact) region on the growth (spallation) side of a transparent polycrystalline diamond sample and (*2*) a fragment ejected from the spallation crater. The spectra are extended along the vertical axis in order to detect weak lines of the non-diamond phase. The inset shows a total Raman spectrum of the same fragment.

sider the volumes of investigated materials as equal. The intensity of the lines of graphite-like carbon on the fragment surface is an order of magnitude higher than for the initial material, and their shape is closer to that observed for the front surface in the ablation crater [17], where diamond is inevitably transformed into graphite as a result of strong heating [17, 18]. This fact indicates partial transformation of diamond on a cleavage plane into a disordered graphite phase during deformation and detachment of diamond layer.

5. Conclusions

The main result of our study is that data on the dynamic strength of poly- and single-crystal diamond targets at high (to 10^8 s^{-1}) strain rates were obtained for the first time. We reached the maximum spall strength of diamond $\sigma^* \approx 16.5$ GPa, which is 24% of the theoretical ultimate strength. It was evidenced that some part of crystalline diamond is graphitised in the spallation region on the rear side of target. Further theoretical and experimental studies must be performed to gain a deeper insight into this phenomenon.

Acknowledgements. This work was supported by the Russian Foundation for Basic Research (Grant Nos 12-02-00625, 12-02-00746, 13-02-91057 and 14-0800967), the Presidium of the Russian Academy of Sciences (Programme Nos 13P 'Extreme Light Fields and Their Applications' and 2P 'Matter under High Energy Densities'), and the RF President's Grants Council (State Support to Leading Scientific Schools Programme, Grant Nos NSh-451.2014.2 and NSh-6614.2014.2).

We are grateful to E.E. Ashkinazi, S.G. Ryzhkov and E.V. Zavedeev for the preparation and profilometry of samples. Electron microscopy of samples was performed by using the equipment of the D.I. Mendeleev Centre for Collective Use.

References

1. Kanel' G.I., Fortov V.E., Razorenov S.V. *Usp. Fiz. Nauk*, **177** (8), 809 (2007).
2. Kanel' G.I., Razorenov S.V., Utkin A.V., Fortov V.E. *Udarnovolnovye yavleniya v kondensirovannykh sredakh* (Shock-Wave Phenomena in Condensed Media) (Moscow: Yanus-K, 1996) p. 408.
3. De Rességuier T., Cuq-Lelandais, J.P., Boustie M., et al., in *Wave Propagation in Materials for Modern Applications* (Croatia: INTECH, 2010) p. 419.
4. Juodkazis S., Nishimura K., Tanaka S., et al. *Phys. Rev. Lett.*, **96**, 166101 (2006).
5. Abrosimov S.A., Bazhulin A.P., Voronov V.V., et al. *Kvantovaya Elektron.*, **43**, 246 (2013) [*Quantum Electron.*, **43**, 246 (2013)].
6. Anisimov S.I., Inogamov N.A., Petrov Y.V., et al. *Appl. Phys. A*, **92** (4), 797 (2008).
7. Zel'dovich Ya.B., Raizer Yu.P. *Fizika udarnykh voln i vysokotemperaturnykh gidrodinamicheskikh yavlenii* (Physics of Shock Waves and High-Temperature Hydrodynamic Phenomena) (Moscow: Fizmatlit, 2008) p. 530.
8. Balmer R.S., Brandon J.R., Clewes C.L., et al. *J. Phys. Condens. Matter*, **21**, 364221 (2009).
9. Mao W.L., Mao H.K., Yan C.S., et al. *Appl. Phys. Lett.*, **83**, 5190 (2003).
10. Ral'chenko V.G., Savel'ev A.V., Popovich A.F., et al. *Mikroelektron.*, **35** (4), 243 (2006).
11. Ralchenko V.G., Pleuler E., Lu F.X., Sovyk D.N., et al. *Diamond Relat. Mater.*, **23**, 172 (2012).
12. McQueen R.G., March D. *J. Appl. Phys.*, **33** (2), 654 (1962).
13. Batani D., Vovchenko V.I., Kanel' G.I., et al. *Dokl. Ross. Akad. Nauk*, **389** (3), 328 (2003).
14. Kulikovskii A.G., Pogorelov N.V., Semenov A.Yu. *Matematicheskie voprosy chislennogo resheniya giperbolicheskikh sistem uravnenii* (Mathematical Problems of Numerical Solution of Hyperbolic Systems of Equations) (Moscow: Fizmatlit, 2012) p. 656.
15. Lomonosov I.V., Fortov V.E., Khishchenko K.V. *Khim Fiz.*, **14** (1), 47 (1995).
16. Vovchenko V.I., Krasyuk I.K., Pashinin P.P., Semenov A.Yu. *Dokl. Akad. Nauk SSSR*, **338** (3), 322 (1994).
17. Kononenko T.V., Ralchenko V.G., Vlasov I.I., et al. *Diamond Relat. Mater.*, **7**, 1623 (1998).
18. Andreev V.D. *Fiz. Tverd. Tela*, **41** (4), 695 (1999).